Applied Physics Letters

631% room temperature tunnel magnetoresistance with large oscillation effect in CoFe/MgO/CoFe(001) junctions

Cite as: Appl. Phys. Lett. **122**, 112404 (2023); https://doi.org/10.1063/5.0145873
Submitted: 08 February 2023 • Accepted: 28 February 2023 • Published Online: 15 March 2023

Thomas Scheike, Zhenchao Wen, Hiroaki Sukegawa, et al.

Applied Physics Letters ARTICLE scitation.org/journal/apl

631% room temperature tunnel magnetoresistance with large oscillation effect in CoFe/MgO/CoFe(001) junctions

Cite as: Appl. Phys. Lett. **122**, 112404 (2023); doi: 10.1063/5.0145873
Submitted: 8 February 2023 · Accepted: 28 February 2023 ·
Published Online: 15 March 2023

Thomas Scheike, Zhenchao Wen, Hiroaki Sukegawa,[a] and Seiji Mitani

AFFILIATIONS

National Institute for Materials Science (NIMS), Tsukuba 305-0047, Japan

[a]Author to whom correspondence should be addressed: SUKEGAWA.Hiroaki@nims.go.jp

ABSTRACT

We demonstrate tunnel magnetoresistance (TMR) ratios of up to 631% at room temperature (RT) using CoFe/MgO/CoFe(001) epitaxial magnetic tunnel junctions (MTJs). The TMR ratio increased up to 1143% at 10 K. The large TMR ratios resulted from fine-tuning of atomic-scale structures of the MTJs, such as crystallographic orientations and MgO interface oxidation by interface insertion of ultrathin CoFe and Mg layers, which are expected to enhance the well-known Δ_1 coherent tunneling transport. Interestingly, the TMR oscillation effect, which is not covered by the standard coherent tunneling theory, also became significant. A 0.32-nm period TMR oscillation with increasing MgO thickness dominates the transport in a wide range of MgO thicknesses; the peak-to-valley difference of the TMR oscillation exceeds 140% at RT, which is attributed to the appearance of large oscillatory components in the resistance area product.

Tunnel magnetoresistance (TMR) effect, which is based on spin-dependent tunneling between ferromagnets (FMs), has been studied in applied physics for over 40 years.[1] It has been extensively investigated from both theoretical and experimental perspectives and has been implemented in practical device applications such as hard disk drives (HDDs) and nonvolatile magnetoresistive random access memories (MRAMs).[2] At present, almost all applications use MgO barrier-based magnetic tunnel junctions (MTJs) due to the large obtainable TMR.[3] The largest experimental TMR ratio at room temperature (RT) is 604%, which was reported in 2008 by Ikeda *et al.*[4] using a pseudo-spin-valve CoFeB/MgO/CoFeB MTJ. However, the progress in the RT-TMR ratio has stagnated over the recent decade. Notably, practical MTJ-based devices can achieve only 100%–200% TMR ratios at best to simultaneously satisfy several requirements for their operation such as circuit impedance matching, high-speed operation, good thermal stability, low power consumption for operation, and low $1/f$ noise at a low frequency range.[5–12]

A major drawback of MTJs as an integrated circuit element is their small current on/off ratio (i.e., small TMR ratio). If much larger RT-TMR ratios can be achieved, the application ranges of TMR-based devices will significantly expand to very high-density MRAMs based on a three-dimensional architecture, nonvolatile magnetic logics,[13] brain-morphic devices,[14] etc. Some of the authors recently investigated simple Fe/MgO/Fe(001) MTJs with a significantly improved TMR ratio up to 417% and 914% at RT and 3 K, respectively, by fine-tuning the crystallinity near the MgO barrier interfaces.[15] A ∼80% peak-to-valley (PV) difference in the RT-TMR ratio oscillation was shown,[15] indicating the dominance of the transport properties by the oscillation effect. Furthermore, a MTJ with a spinel-based $Mg_4Al\text{-}O_x$ barrier, i.e., Fe/$Mg_4Al\text{-}O_x$/Fe(001), showed a similar ∼0.3 nm period oscillation with an enhanced PV difference of ∼125% and a TMR ratio of 429% at RT.[16]

In this Letter, we report on giant TMR effect using CoFe/MgO/CoFe(001) epitaxial MTJs by improving the nanostructures of a MTJ stack. The RT-TMR ratio reached a maximum of 631%, which is the largest RT value reported in MTJs. The significant TMR enhancement was due to the introduction of sub-nm to a few nm CoFe layers at both the top- and bottom-sides of the barrier interface, together with thickness optimization of the Mg insertion at the bottom Fe/MgO interface of the Fe/MgO/Fe(001) framework structure. In addition, we demonstrated a significantly large TMR oscillation with a maximum PV difference of 141% in the CoFe/MgO/CoFe(001) MTJs at RT. Our demonstrations of the large RT-TMR ratio and its oscillatory behavior are crucial steps for developing spintronic applications in the future.

The MTJ stacks were deposited using an ultrahigh-vacuum multichamber deposition apparatus (ULVAC, Inc., base pressure: 4×10^{-7} Pa). Typical stack structures were MgO(001) single crystal substrate//Cr (60)/Fe (50)/$Co_{50}Fe_{50}$ (CoFe) ($d_{bot\text{-}CoFe}$)/Mg (d_{Mg})/wedge-shaped MgO ($d_{MgO} = 1.0 - 3.0$)/natural oxidation/CoFe ($d_{top\text{-}CoFe}$)/Fe (5)/$Ir_{20}Mn_{80}$ (10)/Ru (20) [values in parentheses in nm, see Fig. 1(a)]. All metallic layers were deposited by DC sputtering. The MgO barrier was deposited using electron-beam (EB) evaporation of a sintered MgO pellet and a linear shutter to create the wedge shape for the x-direction of a $20 \times 10\,mm^2$ substrate [see Fig. 1(b)]. After depositing each layer, *in situ* postannealing was performed. More details on the film preparation are described in Ref. 15. The single crystal cubic structures of bottom- and top-Fe electrodes and the MgO barrier were confirmed using reflection high energy electron diffraction (RHEED) observation [Fig. 1(c)]. The multilayer wafers were *ex situ* annealed at 200 °C in a 0.2-T magnetic field along the MgO[110] || Fe[100] || CoFe[100] direction. TMR ratios and resistance area products (RAs) of the wafers were evaluated using the current in-plane tunneling (CIPT) method (Capres A/S, CIPTech-SPM200 prober).[17] From Fig. 1(d), the multilayer was patterned into MTJs with a $10 \times 5\,\mu m^2$ ellipsoidal pillar using photolithography, Ar ion etching, and magnetron sputtering for the SiO_2 insulator and Au electrodes. The magnetotransport properties were characterized by a DC 4-probe method using a sourcemeter (Keithley, 2400) and nanovoltmeter (Keithley, 2182A) at RT and physical property measurement system (Quantum Design, Dynacool) for low temperature (LT) measurements. The TMR ratio is defined as $(R_{AP} - R_P)/R_P \times 100\%$, where R_P [R_{AP}] is the resistance in the parallel (P) [antiparallel (AP)] magnetization state. At positive bias voltage, electrons tunnel from the top to the bottom electrode.

First, we investigated the bottom-CoFe insertion effect using the stack structure shown in the inset of Fig. 2(a), i.e., Fe/CoFe ($d_{bot\text{-}CoFe}$)/Mg/MgO/Fe. In Fig. 2(a), the TMR ratio measured at RT with a bias voltage less than 10 mV as a function of $d_{bot\text{-}CoFe}$ in ML (bottom axis) and nm (top axis) of patterned MTJ pillars is shown. Each TMR ratio is the maximum value for the corresponding wafer. The TMR ratio increases with $d_{bot\text{-}CoFe}$, and it saturates at around 16 ML. The maximum TMR ratio was 504% at $d_{bot\text{-}CoFe} = 24$ ML.

The MgO interfaces were further tuned by controlling the CoFe layer thickness at the top-side ($d_{top\text{-}CoFe}$) and the Mg layer thickness at the bottom-side (d_{Mg}), as shown in the inset of Fig. 2(b), i.e., CoFe (16 ML)/Mg (d_{Mg})/MgO/CoFe ($d_{top\text{-}CoFe}$). Figure 2(b) shows the maximum RT-TMR ratio measured as a function of $d_{top\text{-}CoFe}$. When $d_{top\text{-}CoFe}$ was increased with maintaining $d_{Mg} = 0.5$ nm (green line), the maximum TMR ratio of 551% was observed at $d_{top\text{-}CoFe} = 4$ ML. MTJs with larger $d_{top\text{-}CoFe}$ showed smaller values, indicating that the CoFe insertion effect on the TMR for the top interface differs from that for the bottom one. This behavior is attributable to the difference in their growth mode, which is sensitive to the state of the interfaces, e.g., interfacial roughness, degree of (001)-orientation, and interfacial strain. Figure 2(b) also shows the relationship between the maximum TMR ratio and d_{Mg}. The TMR ratio further increased by optimizing d_{Mg}; the maximum value of 631% at RT was observed at $d_{top\text{-}CoFe} = 4$ ML and $d_{Mg} = 0.6$ nm [black open squares in Fig. 2(b)]. This TMR ratio is larger than the RT-TMR ratio of 604% reported by Ikeda *et al.*[4] using a CoFeB/MgO/CoFeB pseudo-spin-valve MTJ. Therefore, better MgO crystallinity than that of the CoFeB/MgO/CoFeB structure, which requires a high postannealing temperature (525 °C), could be realized at a lower temperature (up to 400 °C) in the epitaxial MTJ in this study. Because the Mg insertion mainly works as protection for the bottom electrode interface from oxidation during the deposition of the MgO barrier and postannealing process in our MTJs, $d_{Mg} = 0.6$ nm is probably the optimum thickness that realizes favorable interface bonding states between CoFe and oxygen atoms at the MgO surface. A lower and higher d_{Mg} reduces the TMR ratio due to slight over- and under-oxidation at the bottom MgO interface, respectively, showing the sensitivity of the bottom interface to the oxidation condition. Notably, for different electrode materials, the optimum Mg insertion thickness may change, e.g., $d_{Mg} = 0.5$ nm for the Fe electrode.[15] Note that the RA decreased slightly when the Mg thickness was increased from 0.5 to 0.6 nm and remained unchanged when further increased to 0.7 nm.

The resistance (left axis) and TMR ratio (right axis) as a function of the magnetic field (H) at RT for the MTJ showing the maximum TMR ratio of 631% ($d_{bot\text{-}CoFe} = 16$ ML, $d_{top\text{-}CoFe} = 4$ ML, $d_{Mg} = 0.6$ nm, and $d_{MgO} = 1.86$ nm) are shown in Fig. 2(c). The curve shows a typical

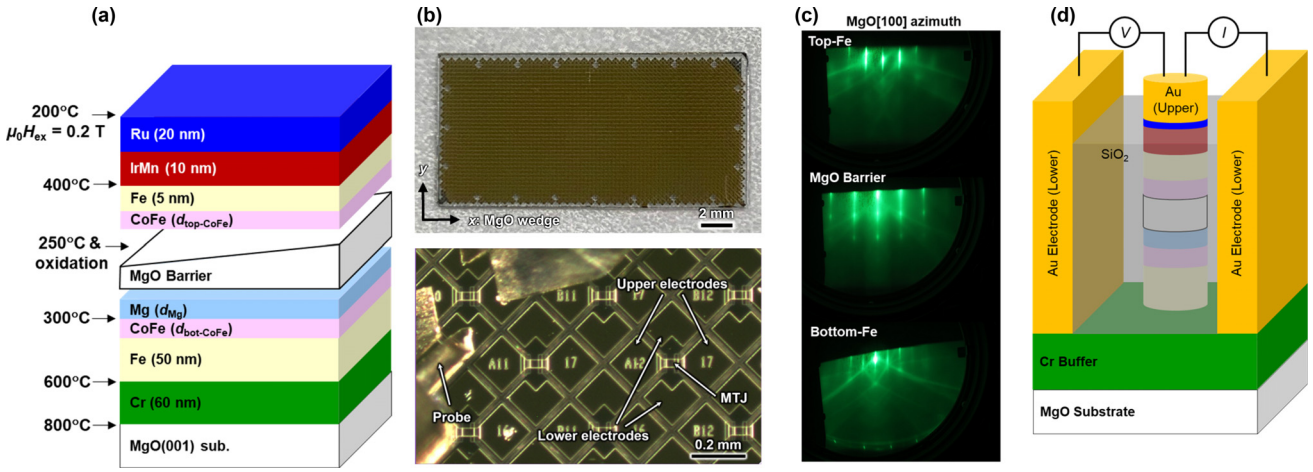

FIG. 1. (a) Schematic MTJ stacking structure and processes. (b) Images of a MTJ wafer. (c) RHEED patterns along the MgO[100] azimuth of top-Fe (upper), the MgO barrier (middle), and bottom-Fe (lower). (d) Schematic structure of a patterned MTJ pillar after microfabrication.

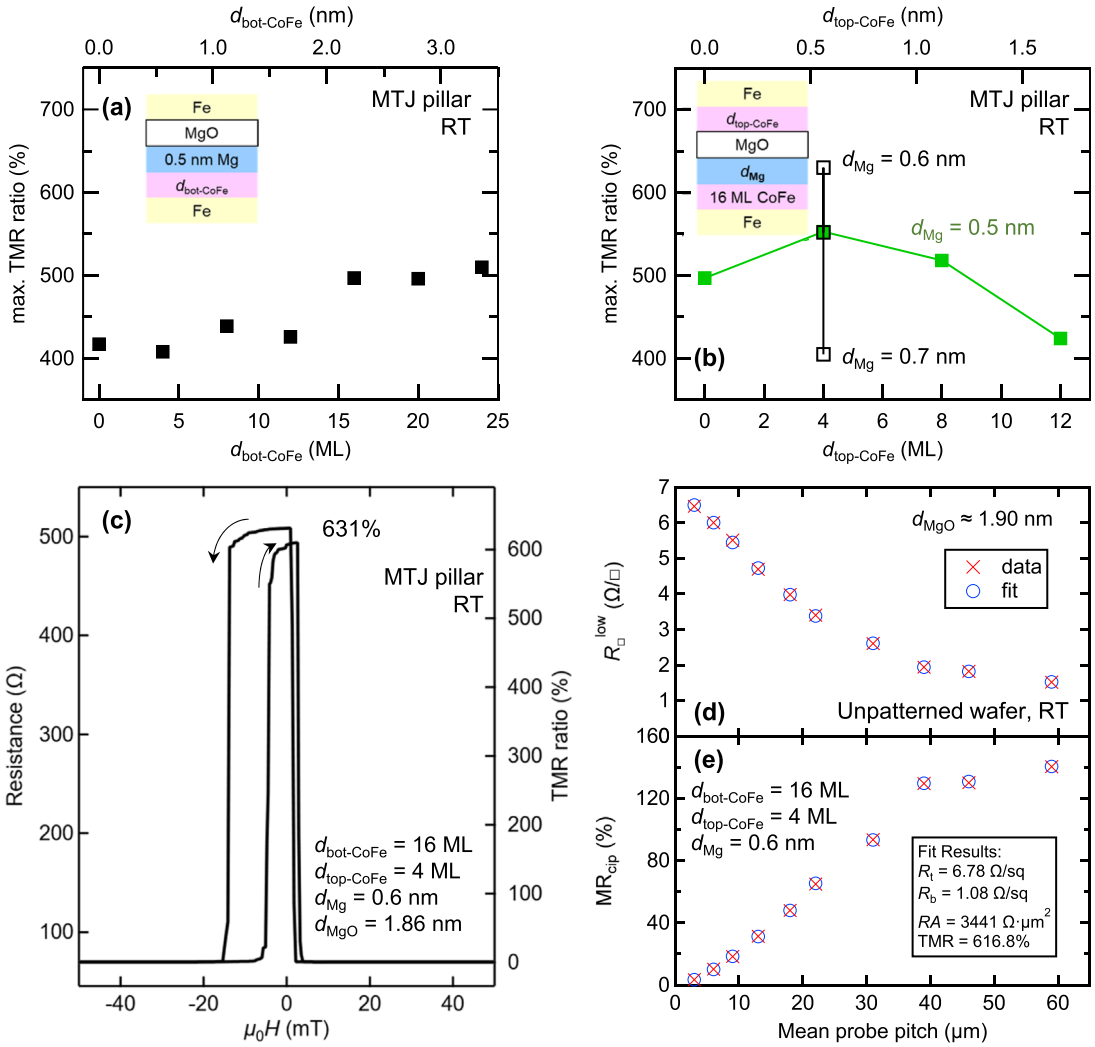

FIG. 2. (a) Maximum RT-TMR ratio vs bottom-CoFe insertion thickness $d_{bot\text{-}CoFe}$. (b) Maximum TMR ratio vs top-CoFe insertion thickness $d_{top\text{-}CoFe}$ and Mg insertion thickness d_{Mg}. Insets of (a) and (b) show schematic stacking structures. (c) Resistance (left axis) and TMR ratio (right axis) vs magnetic field $\mu_0 H$ of a MTJ with maximum RT-TMR ratio ($d_{bot\text{-}CoFe}$ = 16 ML, $d_{top\text{-}CoFe}$ = 4 ML, d_{Mg} = 0.6 nm, and d_{MgO} = 1.86 nm). (d) and (e) CIPT results of the unpatterned wafer of (c); (d) $R_{\square}^{low}$ and (e) MR_{cip}. R_t (R_b) indicates the sheet resistance of the top (bottom) electrode.

exchange-biased hysteresis loop with stable P and AP states at RT. The MTJ has a junction resistance of 70 Ω ($RA = 2.74\,k\Omega{\cdot}\mu m^2$) for the P state, which increases to 7.31 times (=514 Ω) when switched to the AP state. To exclude measurement or microfabrication errors, we also evaluated zero-bias TMR ratios and RA values by CIPT measurements of the unpatterned wafer with $d_{bot\text{-}CoFe} = 16$ ML, $d_{top\text{-}CoFe} = 4$ ML, and $d_{Mg} = 0.6$ nm. Figures 2(d) and 2(e) show the CIPT results near the wafer position of $d_{MgO} = 1.9$ nm: (d) the sheet resistance in the P state ($R_{\square}^{low}$) and (e) the current-in-plane TMR ratio (MR_{cip}) vs the mean probe pitch.[17] The fits (circles) by the theoretical equations match well with the measured data (cross marks). We obtained reasonable values of 617% ($RA = 3.4\,k\Omega{\cdot}\mu m^2$) by the fit. Therefore, the RT-TMR ratio exceeding 600% was confirmed by both an unpatterned wafer (CIPT) and patterned MTJ pillars (DC 4-probe).

Figure 3 shows the temperature dependences of the (a) TMR ratio and (b) R_P and R_{AP} (bias voltage < 10 mV). The corresponding conductance ratio [$= (g_P - g_{AP})/g_P = (R_{AP} - R_P)/R_{AP}$, where $g_{P(AP)} \equiv 1/R_{P(AP)}$ is the DC conductance in the P (AP) state] is also plotted on the right axis. The TMR ratio and conductance ratio monotonically increase with decreasing temperature. The TMR ratio reaches a maximum of 1143% at 10 K, which is much larger than the value of the previous Fe/MgO/Fe (914%)[15] and almost the same as the value of the CoFeB/MgO/CoFeB at LT (1144%) by Ikeda *et al.*[4]

The inset of Figs. 3(a) and 3(b) shows the corresponding TMR-H loop at 10 K. Below 10 K, the TMR ratio reduces slightly because of an imperfect AP state, suggesting that the observed value is underestimated at the LT limit. Using the Julliere model[1] and TMR ratio (%) $= 100 \times 2\ P_{eff}^2/(1 - P_{eff}^2)$, where P_{eff} is the effective spin

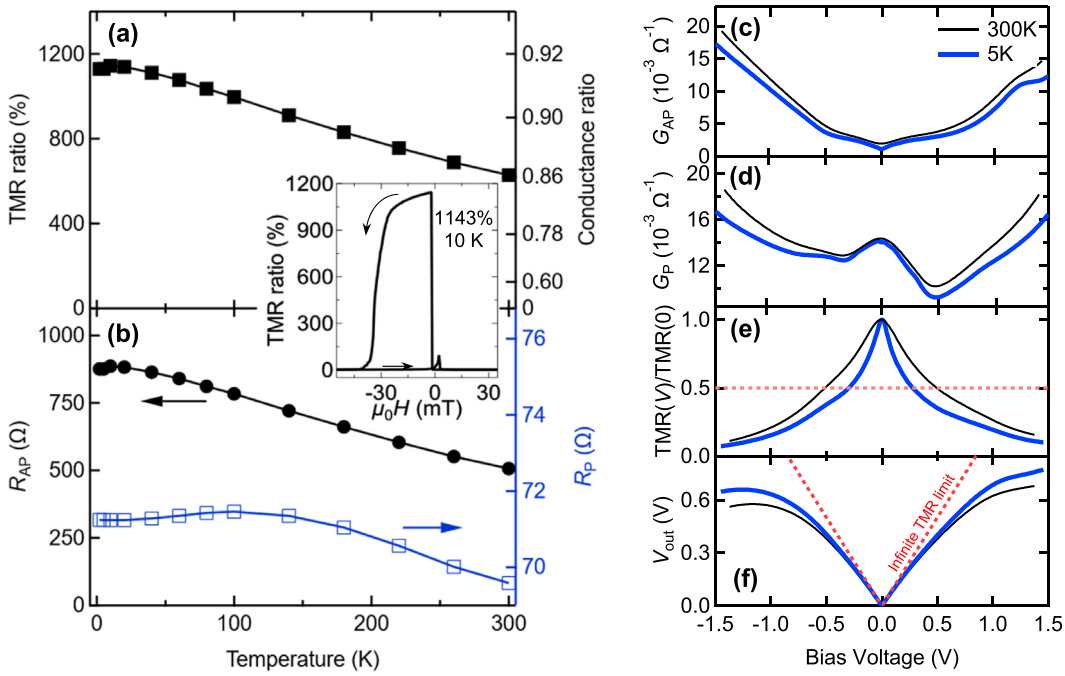

FIG. 3. Temperature dependences of TMR properties of the MTJ with $d_{bot\text{-}CoFe} = 16$ ML, $d_{top\text{-}CoFe} = 4$ ML, $d_{Mg} = 0.6$ nm, and $d_{MgO} = 1.86$ nm. (a) TMR ratio (left axis) and conductance ratio (right axis). (b) R_P (right axis) and R_{AP} (left axis). Inset: TMR ratio vs magnetic field $\mu_0 H$ at 10 K. (c)–(f) Bias voltage dependence measured at 300 K (RT) and 5 K. (c) and (d) Differential conductances G_{AP} and G_P, respectively. (e) TMR normalized by zero-bias value. (f) Output voltage $V_{out} \equiv |V| \times (R_{AP} - R_P)/R_{AP}$.

polarization, P_{eff} at RT (LT) was calculated to be 0.871 (0.923) by assuming both interfaces had the same P_{eff}. The ratio of P_{eff} at RT to LT [P_{eff}(RT)/P_{eff}(LT)] was 0.94, which was higher than 0.91 of previous Fe/MgO/Fe.[15] The weaker temperature dependence is attributable to the increased interface Curie temperature by Co doping into Fe,[18,19] which may effectively improve the interlayer exchange stiffness constant.[20] A recent theoretical work considering an intra-atomic s–d exchange interaction also predicted this improvement in CoFe/MgO/CoFe(001) with an increase in the Co composition.[21] It was also reported for a bcc-Co/MgO/bcc-Co(001) MTJ [P_{eff}(RT)/P_{eff}(LT) = 0.97].[22] Therefore, introducing CoFe at both MgO interfaces effectively suppressed the temperature dependence of P_{eff} in addition to the high P_{eff} at LT, yielding a giant RT-TMR ratio in the present MTJ.

The temperature dependence of the TMR ratio follows that of R_{AP} rather than R_P, which is commonly observed in various MTJs.[23–25] Interestingly, the temperature dependence of R_P shows a complicated behavior with two slope changes, which is different from the dependence of R_{AP} that shows a monotonic change. Similar behavior in R_P has been reported in Co-based electrode MTJs with large TMR ratios such as Co_2(Mn,Fe)Si and Co_2FeAl,[24,25] which contradicts pure Fe electrode MTJs that show a slight monotonic decrease in R_P with decreasing temperature,[15,16,26–28] suggesting a difference in electronic structures between Fe and Co at MgO interfaces.

The bias voltage dependences of the differential conductance for AP (G_{AP}) and P (G_P) at 300 and 5 K are shown in Figs. 3(c) and 3(d), respectively. Figures 3(e) and 3(f) show the bias voltage dependences of the TMR normalized by its zero-bias value and the output voltage V_{out} [$\equiv |V| \times (R_{AP} - R_P)/R_{AP}$, where V is the bias voltage], respectively. The differential conductance G was obtained by the numerical differentiation of current–voltage curves. G_P spectra are asymmetric and have clear minimum structures at −0.3, −0.7, and +0.4 V, which are pronounced at 5 K. The minimum structures in the G_P spectra are larger than those in typical CoFe-based MTJs.[29–31] The minimum structure of the positive bias is much deeper than that of the negative bias; the relative change from the zero-bias value reaches −34% (−29%) at 5 K (300 K). The minimum structures at negative bias are shallower than that at positive bias. However, the appearance of the two minima is similar to the case of the Fe/MgO/Fe(001) MTJs with a large RT-TMR ratio.[15] Tunneling electrons primarily sense the final state, i.e., the top- (bottom-) interface electronic structures at the negative (positive) bias voltage. Thus, the G_P spectra at the negative bias may represent the electronic structure of the top-MgO/CoFe(001) interface, which resembles that of a pure Fe/MgO(001) interface.[15] In contrast, the deep minimum at the positive bias may be associated with specific electronic structures of the bottom-CoFe/MgO(001) interface. These asymmetric features are attributable to the thickness difference of the bottom- and top-CoFe insertion layers (i.e., $d_{bot\text{-}CoFe} = 16$ ML $\gg$ $d_{top\text{-}CoFe} = 4$ ML), implying that further improvement in the RT-TMR ratio can be expected if symmetric spectra are obtained by creating defect-free and well-balanced electronic states between the top- and bottom-side interfaces.

V_{half} values, the bias voltage where the TMR ratio reduces to half of the zero-bias value, at 300 and 5 K for the positive (negative) bias are 0.51 V (−0.49 V) and 0.28 V (−0.30 V), respectively. The curves appear nearly symmetric because of the symmetric G_{AP} feature. The

lower V_{half} compared with Fe/MgO/Fe[32] is mainly due to the CoFe band structure, i.e., the effect of the lowered minority Δ_1 band edge by Co doping into Fe, as seen in bcc-Co/MgO/bcc-Co.[22] V_{out} vs bias voltage shown in Fig. 3(f) is slightly asymmetric with respect to the bias polarity reaching 0.68 V at 300 K (0.77 V at 5 K) at the positive bias region. The value at 300 K is larger than the values reported in CoFeB/MgO/CoFeB MTJs: 0.38[33] and 0.56 V.[34] For our definition, V_{out} at low bias regions nearly follows the line that assumes an infinite TMR (dashed–dotted line) due to the observed large TMR ratio.

Figures 4(a) and 4(b), respectively, show the TMR ratio and *RA* in the P and AP states at RT for the MTJs with $d_{bot\text{-}CoFe} = 16$ ML, $d_{top\text{-}CoFe} = 4$ ML, and $d_{Mg} = 0.6$ nm as a function of d_{MgO} ($|V| < 10$ mV). To obtain consistent plots, we measured the MTJ series along the *x*-direction of the wafer (MgO wedge direction) at the same *y* position [Fig. 1(b)]. From Fig. 4(a), the TMR ratio increased rapidly for $d_{MgO} > 1.2$ nm and showed significant oscillation with d_{MgO}. The oscillation period was approximately 0.32 nm, which was almost identical to the values in Fe/MgO/Fe.[15,35] The maximum PV difference of 141% is larger than previous reports.[32,35,36] Suppression of the oscillation toward a thicker barrier is attributed to the deviation from the optimum interface condition due to the use of the constant $d_{Mg} = 0.6$ nm for the entire wafer. A 0.9-nm period oscillation, which was reported by Matsumoto *et al.*,[35] was not observed in our MTJs.

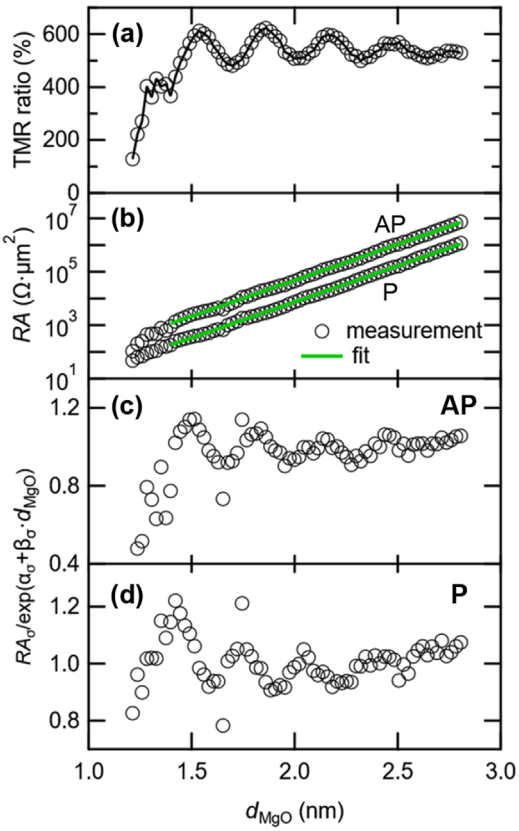

FIG. 4. d_{MgO} dependences of (a) TMR ratio and (b) *RA* for P and AP states at RT. (c) and (d) Background corrected *RA* plots for P and AP states, respectively, with $\sigma = (P, AP)$.

Notably, the significant TMR and *RA* reduction for $d_{MgO} < 1.3$ nm in Fig. 4 is mainly because the MTJ resistances in the low d_{MgO} region (less than a few Ω) are too small to neglect the effect of the electrode resistance (several Ω). In fact, a CIPT result at $d_{MgO} \approx 1.25$ nm ($RA = 69\ \Omega{\cdot}\mu m^2$) showed a TMR ratio of 348%, which is larger than the value of a microfabricated pillar (~270%).

From Fig. 4(b), the plots of ln(*RA*) show a linear increase for both P and AP states in a d_{MgO} range of 1.4–2.8 nm. The oscillatory components of the *RA*s were extracted by the slope-correction of the ln(*RA*) plots.[16,35,37] Here, RA_σ was fitted by $\exp(\alpha_\sigma d_{MgO} + \beta_\sigma)$, where α_σ and β_σ are the fit parameters and $\sigma =$ AP or P. We obtain the slopes $\alpha_P = 6.159$ and $\alpha_{AP} = 6.145\ nm^{-1}$ by fits, indicating that the slopes are nearly identical. Figures 4(c) and 4(d) show the extracted oscillatory components, $RA_\sigma/\exp(\alpha_\sigma d_{MgO} + \beta_\sigma)$, for the AP and P states, respectively. Note that scattering is likely caused by minor damage to the respective MTJ pillar during microfabrication. Both the plots show significant oscillatory behavior with d_{MgO}, which determines the TMR oscillations. Their periods are similar to the previous experimental values for different MTJs with bcc-structured electrodes (0.30 ± 0.02 nm).[32,35] Notably, the oscillations no longer follow a simple sine curve, as observed in the Fe/Mg_4Al-O_x/Fe MTJs.[16]

In summary, we observed a giant TMR ratio of up to 631% (1143%) at RT (10 K) in a CoFe/MgO/CoFe(001) MTJ. The giant value is attributed to improved (001)-orientation and MgO barrier interface crystallinity by introducing ultrathin Mg and CoFe insertion layers and controlling the oxidation states. Furthermore, the observed TMR ratio showed a significant oscillatory behavior as a function of d_{MgO}; the oscillation PV difference reached 141% at RT. The giant TMR ratio and its significant oscillation could be correlated due to common underlying physics. Although we observed a large TMR ratio and its oscillation, asymmetric bias voltage dependences were still observed, indicating that further improvement in the RT-TMR ratio is expected if more symmetric characteristics are achieved by tuning barrier interfaces such as improving the interface crystallinity by nanoinsertions and using the lattice-matched barrier, e.g., $MgAl_2O_4$.

The authors are grateful to Shinji Yuasa for his valuable comments on the TMR oscillation effect of MgO-based MTJs. The authors thank Yoshio Miura and Keisuke Masuda for their fruitful discussion from theoretical viewpoints, and Hiromi Ikeda for her technical support on device microfabrication. This paper is partly based on the results obtained from a Project commissioned by the New Energy and Industrial Technology Development Organization (NEDO) via No. JPNP16007. This work was partly supported by JSPS KAKENHI via Grant Nos. 16H06332, 21H01750, 21H01397, and 22H04966, and the ImPACT Program of the Council for Science, Technology and Innovation (Cabinet Office, Government of Japan).

AUTHOR DECLARATIONS

Conflict of Interest

The authors have no conflicts to disclose.

Author Contributions

Thomas Scheike: Conceptualization (equal); Data curation (lead); Formal analysis (equal); Investigation (lead); Methodology (lead); Visualization (equal); Writing – original draft (lead); Writing –

review & editing (equal). **Zhenchao Wen:** Data curation (supporting); Formal analysis (supporting); Methodology (supporting); Validation (equal); Writing – original draft (supporting); Writing – review & editing (supporting). **Hiroaki Sukegawa:** Conceptualization (lead); Funding acquisition (lead); Investigation (supporting); Methodology (equal); Supervision (lead); Validation (lead); Visualization (supporting); Writing – original draft (equal); Writing – review & editing (lead). **Seiji Mitani:** Funding acquisition (lead); Methodology (supporting); Supervision (equal); Writing – review & editing (equal).

DATA AVAILABILITY

The data that support the findings of this study are available from the corresponding author upon reasonable request.

REFERENCES

[1]M. Julliere, Phys. Lett. A **54**, 225 (1975).
[2]H. J. M. Swagten, in *Handbook of Magnetic Materials* (Elsevier, 2007), pp. 1–121.
[3]S. Yuasa and D. D. Djayaprawira, J. Phys. D **40**, R337 (2007).
[4]S. Ikeda, J. Hayakawa, Y. Ashizawa, Y. M. Lee, K. Miura, H. Hasegawa, M. Tsunoda, F. Matsukura, and H. Ohno, Appl. Phys. Lett. **93**, 082508 (2008).
[5]A. V. Silva, D. C. Leitao, J. Valadeiro, J. Amaral, P. P. Freitas, and S. Cardoso, Eur. Phys. J. Appl. Phys. **72**, 10601 (2015).
[6]K. Yakushiji, A. Sugihara, A. Fukushima, H. Kubota, and S. Yuasa, Appl. Phys. Lett. **110**, 092406 (2017).
[7]S. Bhatti, R. Sbiaa, A. Hirohata, H. Ohno, S. Fukami, and S. N. Piramanayagam, Mater. Today **20**, 530 (2017).
[8]M. Romera, P. Talatchian, S. Tsunegi, F. Abreu Araujo, V. Cros, P. Bortolotti, J. Trastoy, K. Yakushiji, A. Fukushima, H. Kubota, S. Yuasa, M. Ernoult, D. Vodenicarevic, T. Hirtzlin, N. Locatelli, D. Querlioz, and J. Grollier, Nature **563**, 230 (2018).
[9]A. Hirohata, K. Yamada, Y. Nakatani, I.-L. Prejbeanu, B. Diény, P. Pirro, and B. Hillebrands, J. Magn. Magn. Mater. **509**, 166711 (2020).
[10]A. Fukushima, T. Yamamoto, T. Nozaki, K. Yakushiji, H. Kubota, and S. Yuasa, APL Mater. **9**, 030905 (2021).
[11]S. Jung, H. Lee, S. Myung, H. Kim, S. K. Yoon, S.-W. Kwon, Y. Ju, M. Kim, W. Yi, S. Han, B. Kwon, B. Seo, K. Lee, G.-H. Koh, K. Lee, Y. Song, C. Choi, D. Ham, and S. J. Kim, Nature **601**, 211 (2022).
[12]G. Albuquerque, S. Hernandez, M. T. Kief, D. Mauri, and L. Wang, IEEE Trans. Magn. **58**, 1 (2022).
[13]N. Maciel, E. Marques, L. Naviner, Y. Zhou, and H. Cai, Sensors **20**, 121 (2019).
[14]D. Ielmini and S. Ambrogio, Nanotechnology **31**, 092001 (2020).
[15]T. Scheike, Q. Xiang, Z. Wen, H. Sukegawa, T. Ohkubo, K. Hono, and S. Mitani, Appl. Phys. Lett. **118**, 042411 (2021).
[16]T. Scheike, Z. Wen, H. Sukegawa, and S. Mitani, Appl. Phys. Lett. **120**, 032404 (2022).
[17]D. C. Worledge and P. L. Trouilloud, Appl. Phys. Lett. **83**, 84 (2003).
[18]I. Ohnuma, H. Enoki, O. Ikeda, R. Kainuma, H. Ohtani, B. Sundman, and K. Ishida, Acta Mater. **50**, 379 (2002).
[19]M. A. Turchanin, L. A. Dreval, A. R. Abdulov, and P. G. Agraval, Powder Metall. Met. Ceram. **50**, 98 (2011).
[20]Y. Miura, K. Abe, and M. Shirai, Phys. Rev. B **83**, 214411 (2011).
[21]K. Masuda, T. Tadano, and Y. Miura, Phys. Rev. B **104**, L180403 (2021).
[22]S. Yuasa, A. Fukushima, H. Kubota, Y. Suzuki, and K. Ando, Appl. Phys. Lett. **89**, 042505 (2006).
[23]S. G. Wang, R. C. C. Ward, G. X. Du, X. F. Han, C. Wang, and A. Kohn, Phys. Rev. B **78**, 180411 (2008).
[24]B. Hu, K. Moges, Y. Honda, H. Liu, T. Uemura, M. Yamamoto, J. Inoue, and M. Shirai, Phys. Rev. B **94**, 094428 (2016).
[25]T. Scheike, H. Sukegawa, T. Ohkubo, K. Hono, and S. Mitani, J. Phys. D **53**, 045001 (2020).
[26]S. S. P. Parkin, C. Kaiser, A. Panchula, P. M. Rice, B. Hughes, M. Samant, and S.-H. Yang, Nat. Mater. **3**, 862 (2004).
[27]E. Y. Tsymbal and I. Zutic, *Handbook of Spin Transport and Magnetism* (CRC Press, 2011).
[28]M. Belmoubarik, H. Sukegawa, T. Ohkubo, S. Mitani, and K. Hono, Appl. Phys. Lett. **108**, 132404 (2016).
[29]S. Ikeda, J. Hayakawa, Y. M. Lee, T. Tanikawa, F. Matsukura, and H. Ohno, J. Appl. Phys. **99**, 08A907 (2006).
[30]V. Drewello, M. Schäfers, O. Schebaum, A. A. Khan, J. Münchenberger, J. Schmalhorst, G. Reiss, and A. Thomas, Phys. Rev. B **79**, 174417 (2009).
[31]F. Bonell, T. Hauet, S. Andrieu, F. Bertran, P. Le Fèvre, L. Calmels, A. Tejeda, F. Montaigne, B. Warot-Fonrose, B. Belhadji, A. Nicolaou, and A. Taleb-Ibrahimi, Phys. Rev. Lett. **108**, 176602 (2012).
[32]S. Yuasa, T. Nagahama, A. Fukushima, Y. Suzuki, and K. Ando, Nat. Mater. **3**, 868 (2004).
[33]D. D. Djayaprawira, K. Tsunekawa, M. Nagai, H. Maehara, S. Yamagata, N. Watanabe, S. Yuasa, Y. Suzuki, and K. Ando, Appl. Phys. Lett. **86**, 092502 (2005).
[34]G. Feng, S. van Dijken, J. F. Feng, J. M. D. Coey, T. Leo, and D. J. Smith, J. Appl. Phys. **105**, 033916 (2009).
[35]R. Matsumoto, A. Fukushima, T. Nagahama, Y. Suzuki, K. Ando, and S. Yuasa, Appl. Phys. Lett. **90**, 252506 (2007).
[36]T. Ishikawa, S. Hakamata, K. Matsuda, T. Uemura, and M. Yamamoto, J. Appl. Phys. **103**, 07A919 (2008).
[37]T. Marukame, T. Ishikawa, T. Taira, K. Matsuda, T. Uemura, and M. Yamamoto, Phys. Rev. B **81**, 134432 (2010).